Langmuir

Article

pubs.acs.org/Langmuir

Assessment of the Nature Interactions of β-Amyloid Protein by a Nanoprobe Method

Leonardo Caballero,[†] Juan Mena,[†,‡] Aurora Morales-Alvarez,[‡] Marcelo J. Kogan,*[,‡] and Francisco Melo*[,†]

[†]Departamento de Física, Universidad de Santiago, Avenida Ecuador 3493, Casilla 307, Correo 2, Santiago, Chile

[‡]Facultad de Ciencias Químicas y Farmacéuticas and Advanced Center for Chronic Diseases (ACCDiS), Universidad de Chile, Santos Dumont 964, Independencia, Santiago, Chile

ABSTRACT: We present a method based on atomic force microscopy (AFM) to assess the work of adhesion between the interfaces of gold AFM tips functionalized with three peptides derived from β-sheet breaker LPFFD [CLPFFD-NH_2 (i_0) and their isomers CDLPFF-NH_2 (i_1) and CLPDFF-NH_2 (i_2)], and the beta-amyloid protein ($A\beta_{1-42}$). β-Amyloid protein was deposited onto a highly oriented graphite (HOPG) surface as protofibrils and fibrils. The presence of the residues Leu (L), Phe (F), and Phe (F), which are also present in the native sequence, confirm that the peptides are able to bind to the aggregates of $A\beta_{1-42}$ fibrils and protofibrils. Force of adhesion data were directly obtained from the maximum force on retraction, and the work of adhesion was calculated from the Jhonson−Kendall−Roberts model (JKR-Model). Both the polar and dispersive contributions to the surface energy of the peptides i_0, i_1, and i_2, as well as $A\beta_{1-42}$ fibrils and protofibrils, were determined by means of measuring the contact angle and using the two-fluid method. The macroscopic energies of the functionalized gold surfaces do not differ significantly between isomers, which confirms the similar nature of the peptides i_0, i_1, and i_2 but suggests that the macroscopic measurements are not able to distinguish specific sequences. The nanoprobe reveals a typical adhesion work value associated with the interaction of protofibrils with i_0 and i_2; this value is three times higher than that of i_1. The difference is attributed to the hydrophobic nature of protofibrils, the predominant exposition of hydrophobic residues of the peptides i_0 and i_2, with respect to i_1, and the degree of functionalization. i_0 and i_2 presented a slight adhesion with Aβ fibrils, which is associated with the exposed hydrophilic groups of these fibrils (onto HOPG) compared to the protofibrils. However, i_1 showed interaction with both Aβ fibrils and protofibrils. For this, we propose an explanation based on the fact that the peptide i_1 locates itself adjacent to the gold surface of the probe, concealing their hydrophobic groups and therefore decreasing the probability of interaction with Aβ fibrils and protofibrils. The peptide−gold nano probe represents a useful tool to study the nanobiointeractions of functionalized nanoparticles with amyloid aggregates.

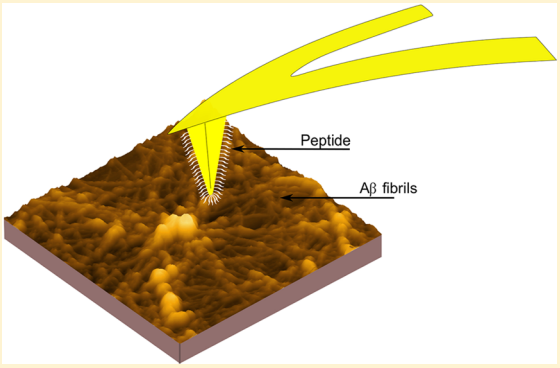

INTRODUCTION

The intermolecular forces acting at interfaces on a nanometer scale play a key role in a wide range of chemical, biological, and physical processes,[1−3] including chemical and physical absorption, wetting, wear, catalysis, adhesion, and cell recognition. The interactions involved, especially when measured in a liquid environment, can be mostly explained in terms of van der Waals forces, electrostatic Coulombic interactions, solvation forces, and hydrogen bonding.[1,4,5] The use of thiol chemistry and the strong covalent S−Au bonding allow for the formation of self-assembled monolayers with different functionalities on gold-coated cantilevers. Thus, the interaction forces between a chemically derivatized surface and the tip are directly related to their respective chemical composition. Hence, this methodology, referred to as chemical force microscopy, has been applied to study the interactions between proteins and ligands. When the surface, the tip, or both surfaces are functionalized with an ionizable group, the method has been referred to as force titration.[6] Force spectroscopy (FS), based on atomic force microscopy (AFM), has also been developed and can be applied to study different processes in proteins,[7] especially in the single-molecule mode using functionalized tips. Through the application of single-molecule testing methods, it has been possible to obtain important insights into various biomolecular systems that would be otherwise unavailable.[7−9] A noteworthy application of this method is the study of the mechanical properties of the β-amyloid protein using single-molecule manipulation approaches,[10] which can be relevant to understand the molecular basis of Alzheimer's disease (AD). The Aβ peptide is the most common cause of dementia, which affects more than 34 million people worldwide. It is characterized by the presence of dense extraneuronal protein deposits (amyloid plaque) and intraneuronal fibrous features (neurofibrillary

Received: July 21, 2014
Revised: September 29, 2014
Published: December 8, 2014

tangles).[11] Amyloid plaques are formed by a wide variety of substances with Aβ as the main constituent. The aggregation of Aβ is closely related to neurodegeneration and the development of AD.[11] The use of a synthetic Aβ has facilitated *in vitro* assays and the study of the complex aggregation/antiaggregation processes. Lesne[11] and Cohen[12] have reviewed commonly used techniques in the study of amyloid self-assembly and described their limitations. Previously, we have also reported the value of AFM and transmission electron microscopy (TEM) for qualitative kinetic purposes[13] when examining morphological development over time. Nanoparticles can influence fibrillation processes of amyloids, depending on the particle size and surface functionality.[14] Amyloid fibrillation is accelerated by different nanomaterials as carbon nanotubes, cerium oxide,[15] TiO_2 nanoparticles,[16] polymer-coated quantum dots,[17] polymer particles, anionic gold nanoparticles (AuNP),[18,19] anionic quantum dots,[20] α-synuclein-functionalized quantum dots, and peptide-functionalized ferric oxide nanoparticles.[21] In contrast, retardation of amyloid fibrillation has been reported for hydrophobic polymer nanoparticles,[22] *N*-acetyl-lcysteine-capped CdTe quantum dots,[23] thioglycolic acid-capped CdTe quantum dots,[24] dihydrolipoic acid capped CdSe/ZnS quantum dots,[25] and fetal-bovine-serum-coated graphene oxide.[26] Thioflavin S-conjugated graphene oxide has been used to dissolve amyloid fibrils under photothermal conditions.[27] Anionic AuNP and curcumin AuNP have also been shown to induce fibril dissociation.[28,29]

In our group, we conjugated a peptide derived from the sequence LPFFD-NH_2, which is a well-known β-amyloid aggregation inhibitor and a fibril disruptor designed by Soto et al.[30] to spherical AuNP or to gold nanorods to destroy Aβ aggregates by using microwaves or photothermal conditions, respectively.[31,32] The designed peptide LPFFD is derived from the original sequence of Aβ which contain amino acids 17−20 (LVFF) in the central hydrophobic region in the N-terminal domain which served as a design template for the β-sheet breaker peptide LPFFD. Amino acid substitutions in this region of Aβ substantially alter the peptide conformation and its capacity to produce fibrils; therefore, this small fragment could block the aggregation process.[33]

The aforementioned findings related with the use of nanoparticles for disaggregation of amyloids suggest that a nanoparticle-based approach might be a promising option for the treatment of various neurodegenerative diseases. However, although the effects of nanoparticles are well documented their nanobiointeractions with amyloids are not well understood. This is crucial to control the effects of functionalized nanoparticles on β-amyloid aggregates, which is very relevant for the reliable use of nanoparticles for diagnosis and therapy of AD.

In a previous study, we explored surface charge presence and peptide conformation on AuNP functionalized with CLPFFD-NH_2 (i_0), and with their isomers CDLPFF-NH_2 (i_1) and CLPDFF-NH_2 (i_2), using several methodologies including the colloidal probe technique.[34,35] In the case of i_1, the peptide molecules are positioned horizontally on the surface exposing all groups to the environment. In the case of i_0 and i_2, the peptide molecules extend nearly orthogonally to the surface that exposes the aspartic polar residue D and the phenylalanine residues F (i_2), respectively. These features of the peptide molecules on the surface of AuNPs can be used to design tailored nanoprobes that combine atomic force measurements with gold tips functionalized with three distinct peptides. Here, we show the benefit of using nanoprobes to study the adhesion or affinity of molecules that interact with Aβ, which is useful information to explain the interaction of nanoparticles with amyloid aggregates. This article aims to characterize the interaction of peptide functionalized AuNPs with Aβ. To mimic such interactions, we assess the force of adhesion necessary to pull AFM tips, of 30 nm radius functionalized with peptides (i_0, i_1, i_2), from a nanometric film formed by either Aβ fibrils or protofibrils. In order to compare our results with the macroscopic measurements of interaction involved in such interfaces, we first determined the average surface energy through the wetting angle method and two fluid methodology. We determined the polar and dispersive contributions to the surface energy of β-sheet breakers onto a gold substrate, as well as Aβ fibrils and protofibrils onto a highly ordered pyrolytic graphite (HOPG) substrate. The macroscopic energies of the functionalized surfaces did not differ significantly between isomers, confirming the similar nature of the isomeric peptides but suggesting that the macroscopic measurements do not distinguish their particular sequence.

In turn, the nanoprobe method along with the Jhonson−Kendall−Roberts model (JKR-Model)[3] revealed values of adhesion work, associated with the interaction of protofibrils with i_0 and i_2. We showed that these values are three times higher than those of i_1. We attributed this difference to the hydrophobic nature of protofibrils and the predominant exposition of the hydrophobic residues of i_0 and i_2, as the peptides are positioned orthogonally to the surface, whereas in i_1 the hydrophobic groups are adsorbed on the gold surface. Peptides i_0 and i_2 presented a slight adhesion with Aβ fibrils, which is associated with the hydrophilic nature of these fibrils (onto HOPG) with respect to protofibrils. However, i_1 revealed a non-negligible work of adhesion with both Aβ fibrils and protofibrils.

Thus, our findings demonstrate that peptide sequences affect the interaction of the AuNP peptide conjugate with Aβ fibrils and protofibrils. The peptide sequence, the steric effects, and the charge and disposition of hydrophilic and hydrophobic residues are important parameters for nanobiointeractions. In addition, the force of adhesion of the nanoparticles to the Aβ-fibrils on the surface can be significantly affected by the fibril orientation, decreasing their efficiency in potential biomedical applications such as drug delivery and localized heating treatment.

EXPERIMENTAL METHODS

Growth of Aβ_{1-42} Fibrils. Aβ_{1-42} ultrapurified in HFIP (1,1,1,3,3,3-hexafluoro-2-propanol; 99,8) was obtained from r-Peptide Company (Bogarta, CA). Initially, a 0.05 mg aliquot of the product was resuspended in 200 μL of HFIP and lyophilized overnight. The resulting mass of Aβ_{1-42} peptide monomers was then dissolved in 7.5 μL of 1 mM NaOH and 12.5 μL of 10 mM NaOH. Then, 90 μL of 20 mM phosphate buffer, pH 7.4 (0.1 M NaH_2PO_4 and 0.1 M Na_2HPO_4) was added, which resulted in a final concentration of 92 μM Aβ_{1-42} monomer. All solutions were freshly prepared using ultrapure Milli-Q water (Diret-Q Millipore system) and filtered through a 0.2 μm cellulose acetate filter. Subsequently, the solution was incubated at 37 °C for 20 h in an Eppendorf Thermomixer Comfort incubator. The same protocol was used to prepare Aβ_{1-42} protofibrils; however, the temperature and the incubation times were adjusted to 25 °C and 24 h, respectively.

AFM Imaging. An aliquot of the final Aβ_{1-42} fibril solution was adjusted to pH 9 using 0.1M NaOH. NaCl was added to attain a salt concentration of 140 μM. For air images, this sample was deposited

dx.doi.org/10.1021/la502777h | *Langmuir* 2015, 31, 299−306

onto freshly cleaved HOPG for 15 min, and the surface was washed with 20 mM phosphate buffer to remove excess of Aβ_{1-42} fibrils.

AFM imaging of samples and adhesion force measurements were carried out using a NanoScope IIIa Multimode atomic force microscopy device with scanner types "*E*" and "*J*", from Digital Instruments Inc., California. Silicon nitride cantilevers, TR400PB models (Asylum Research Inc.), were used, with gold coating on both the tip and the reflected side, and a spring constant of approximately 0.05 N/m. Images in fluid were taken using the Fluid Tapping Mode with a tapping frequency ranging from 7 to 9 kHz, an image resolution of 256 × 256 pixels, and a scan rate of 1 Hz. For air tapping mode, the tapping frequency ranged from 70 to 75 kHz, and the scan rate was 1 Hz with an image resolution of 512 × 512 pixels.

Cantilever Functionalization. Gold coated silicon nitride cantilevers were functionalized with each isomer as follows: first, the cantilever was submerged in newly prepared piranha solution at 30% dissolution (H_2O_2/H_2SO_4, 1/3 in volume) for 5 min. The cantilever was then washed in abundant Milli-Q water and dipped in the correspondent isomer solution of 100 nM concentration for several seconds. Longer periods of contact between the naked gold cantilever and the isomer solution did not significantly change our results.

Force Measurements. In order to measure force adhesion in HOPG, Aβ_{1-42} fibrils, and protofibrils, samples were prepared following AFM imaging methodology. The peptide functionalized gold cantilevers were prepared as previously explained and used immediately after functionalization. The spring constant of functionalized cantilevers was determined by thermal noise methodology prior to functionalization.[36] Post-experimentation, the elastic constant of the cantilevers did not change significantly. Radii of curvature of the functionalized tips were determined by analysis of scanning electron microscope (SEM) images and ranged from 30 to 37 nm. To ensure regular or total cover of either fibrils or protofibrils on the surface, a low resolution image scan was performed before each session of force curves acquisition. This inspection was performed in a fluid environment and allowed one to select well covered regions for adhesion evaluation. Withdraw force data were obtained automatically in a 10 × 10 grid and taken at 50 nm steps, for both columns and rows, with a scan rate of 0.3−0.6 Hz. Each force curve was recorded by sensing the cantilever deflection due to the sample tip interaction. At each point of the grid, a single force curve is obtained, which provides 100 data points curved by a grid. This force acquisition procedure was repeated for a minimum of 8 grids, which provided us with enough data to obtain representative statistics of the adhesion force.

Contact Angle Measurement. Sample preparation for contact angle measurements was achieved as follows.

Fibril and Protofibril Substrate Preparation. A 100 μL aliquot of the corresponding Aβ_{1-42} fibril or protofibril sample was deposited onto a freshly cleaved HOPG surface and left to dry overnight. Afterward, the surface was washed by depositing 300 μL of Milli-Q water on the surface for 1 h to ensure total dilution of the remaining salt.

Gold Substrata Preparation. For gold surface preparation, commercial silicium wafers were used as primary substrata. Small pieces (12 × 12 mm^2) cut from wafers are first cleaned with abundant isopropanol and maintained under piranha solution (H_2O_2/H_2SO_4, 1/3 in volume) for 24 h to remove organic residues. Abundant Milli-Q water and clean nitrogen were used for substrata rinsing and drying, respectively. To improve adhesion, metal evaporation performed at 10^{-8} bar is used to deposit a thin chrome layer (1−2 nm thick). The resulting gold layer, 60−70 nm thick, is immediately deposited using the same procedure. Gold layer roughness was about 1 nm. The quoted value of roughness corresponds to the variance of the surface height calculated directly from the profiles provided by AFM images of 4 × 4 μm^2 area. Typical lateral size of roughness is about 70 nm.

Gold Surface Functionalized with (i_0) and with Their Isomers (i_1) and (i_2). Immediately after gold deposition, gold substrata were washed in abundant Milli-Q water and dipped into the corresponding isomer solution of 100 nM concentration for about 30 s. Abundant Milli-Q water and clean Nitrogen were used for substrata rinsing and drying, respectively.

Contact Angle. Immediately after the deposition of Aβ fibrils/protofibrils or functionalization with peptides, a 0.5 μL droplet of either Milli-Q water or diiodomethane was set in the center of the HOPG or gold samples Lateral images of droplets were digitally captured using a 10× optic fiber microscope for assessment of contact angles and further analysis by computer software.

RESULTS AND DISCUSSION

Imaging Protofibrils and Fibrils on a HOPG Substrate.

As previously described, for protofibril formation, Aβ_{1-42} samples were incubated for 24 h at 25 °C and deposited onto a freshly cleaved HOPG substrate. Control images were instead obtained in both air and fluid environments using the tapping mode, although they do not differ significantly. While tapping mode in air produced better quality images, tapping in fluid proved very useful to ensure control sample homogeneity prior to the nanoprobe assay. In air, protofibrils are observed at relatively low magnification to be organized in regular patches (Figure 1a). However, higher magnifications reveal the

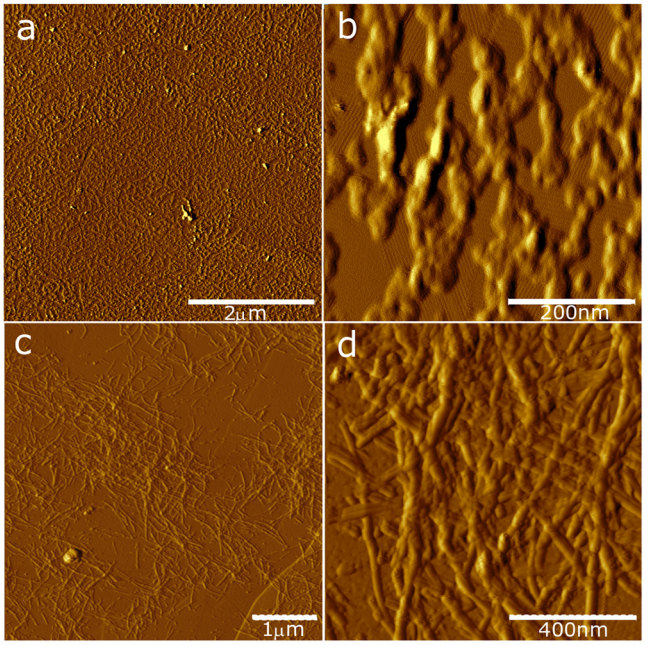

Figure 1. Control images illustrating the coverage of Aβ_{1-42} protofibrils and fibrils at different amplifications. Upper panels a and b: Aβ_{1-42} protofibrils. Lower panels c and d: Aβ_{1-42} fibrils as seen by an atomic force microscope.

occurrence of protofibril structures which tend to align regularly, forming bundles of several units (Figure 1b). Occasionally, straight protofibrils oriented in 6-fold symmetry were distinguished on the film. It is suggested that this kind of pattern is a result of the crystal structure of graphite that would act as a template to orient certain molecules along three directions at 60° to one another.[37] Such template-directed assembly induced by the hexagonal graphite lattice has also been described for the β-sheet containing *de novo* designed protein.[38]

Relatively higher temperatures favor fibril development; therefore, samples were incubated for 24 h at 37 °C. Abundant fibrils with a mean width of 11.4 ± 0.8 nm (30.1 ± 7.7 nm before deconvolution) and height of about 5 nm were observed in Aβ_{1-42} preparations; see Figure 1c and d. Examples

dx.doi.org/10.1021/la502777h | *Langmuir* 2015, 31, 299−306

Table 1. First Two Columns Indicate the Average Contact Angle for Water and Diiode-methane, Respectively, while the Two Last Columns to the Right Indicate the Work of Adhesion of the Substrata and Water and Diiode-Methane, respectively

← contact-angle / deg			adhesion-work / mJ/m^2 →	
water	diiode-methane		water	diiode-methane
86 ± 3	21 ± 4	HOPG	77(62.6[41])	98.2(97.9[41])
40 ± 5	40 ± 2	HOPG-Aβ	127	89.7
57 ± 5	33 ± 3	HOPG-protofibrils	111	93.4
89 ± 3	25 ± 2	Au/i_0	73.3	96.8
89 ± 4	15 ± 2	Au/i_1	73.3	100
90 ± 3	20 ± 3	Au/i_2	72	98.5

demonstrating dense coverage of fibrils, as illustrated in Figure 1d, were selected to assess local adhesion.

Surface Adhesion: Contact Angle Method. Several techniques have become widely used to assess the surface energy for various materials; these are based on the measurement of the wetting angle made by different fluids with the surface under investigation. In terms of polar interactions, both the advantages and disadvantages of such methods, as well as their domain of applicability, have been discussed recently by Carré.[39] The polar and dispersive contributions of inorganic materials interacting with high energy surfaces have been investigated by Ho Cho[40] using two fluids of well-known polar and dispersive components. Additionally, Wang[41] presents a similar method for the assessment of the adhesion work of graphene and graphite.

For a macroscopic characterization of the interaction between the surfaces functionalized with peptides and Aβ fibrils and protofibrils, we applied the two fluids method. We use as testing fluids water and diiodo-methane. This choice provides both the polar and the dispersive contribution of the surfaces involved in our investigation. To write some useful relationships, we assume the same conditions as those given by Young's equation. Therefore, the contact angle, θ_{SL}, relates to the surface energy as,

$$\gamma_S = \gamma_{SL} + \gamma_L \cos\theta_{SL} \tag{1}$$

where the subscripts S and L indicate the solid and the fluid surface, respectively. The work of adhesion is the decrease in the Gibbs free energy per unit area when two new surfaces are formed while the interfacial area disappears. The equation for the adhesion work of a solid surface in contact with a liquid is as follows:

$$W_{SL} = \gamma_S + \gamma_L - \gamma_{SL} \tag{2}$$

Combining eq 1 with eq 2 we obtain

$$W_{SL} = \gamma_L(1 + \cos\theta_{SL}) \tag{3}$$

which relates the work of adhesion to the contact angle. The average contact angles for the substrata of interest were measured, and the results are summarized in Table 1. The work of adhesion obtained from eq 3 is also presented in Table 1.

Conversely, for low energy surfaces it is suitable to express the work of adhesion as the geometric means of the dispersive component of the surface energies. An analogous geometric mean can be employed to account for the polar component, which leads to

$$W_{12} = 2\sqrt{\gamma_1^p\gamma_2^p} + 2\sqrt{\gamma_1^d\gamma_2^d} \tag{4}$$

where we assumed that $\gamma_i = \gamma_i^d + \gamma_i^P$, with i = 1,2. Our testing fluids (water and diiodo-methane) are labeled as (W) and (D),

Table 2. Dispersive and Polar Contributions of the Substrate Investigated in the Present Work[a]

surface energy (mJ/m^2)	$\gamma = \gamma^d + \gamma^p$	γ^d	γ^p	γ_{sw}
water (W)	71.8	21.8	50	
diiode-methane (D)	50.8	50.8	0	
HOPG	48.5(54.8[41])	47.5	1	43.3
HOPG-Aβ	63	39.6	23.4	2.3
HOPG-protofibrils	56.1	43	13.1	16.9
Au/i_0	46.7	46.1	0.6	45.4
Au/i_1	49.4	49	0.4	47.4
Au/i_2	48.3	47.8	0.5	47.6

[a]The first two rows indicate the dispersive and polar contributions of the reference fluids used for testing energy surfaces. The last column indicates the values of solid−water surface energy, γ_{sw} as calculated from eq 1.

and their polar and dispersive contributions are summarized in Table 2. Moreover, in the two fluid method, combining eq 3 with eq 4, a set of two equations can be written:

$$\gamma_W(1 + \cos\theta_{SW}) = 2\sqrt{\gamma_W^p\gamma_S^p} + 2\sqrt{\gamma_W^d\gamma_S^d} \tag{5}$$

$$\gamma_D(1 + \cos\theta_{SD}) = 2\sqrt{\gamma_D^p\gamma_S^p} + 2\sqrt{\gamma_D^d\gamma_S^d} \tag{6}$$

where S generically represents a specific solid surface. In the following, we extracted the polar and dispersive components of distinct peptides, as well as of Aβ protein, from eqs 5 and 6. The results, which are summarized in Table 2, indicate that the peptide functionalized gold surface is similar to naked HOPG with respect to polar and dispersive components. It seems that in this type of peptide surface the interaction is dominated by the dispersive component only. Interestingly, polar and dispersive components do not differ between peptides, probably due to the similar structure of peptides regardless of their conformation and sequence. In turn, for Aβ surfaces (Aβ onto HOPG) while the dispersive component remains of the same order, the polar component becomes about one-half of the dispersive one. Similar behavior is observed for protofibril surfaces, although the polar component is slightly smaller, at about one-third of the dispersive one.

Direct Measurement of Adhesion: Interaction of the Peptide Functionalized Tips with Aβ Fibrils and Protofibrils. The contact angle method previously presented provides the average values of the surface energy of the systems under investigation. Aiming to characterize our system at the nanometric scale, we directly measure the adhesion force involved when pulling a suitable functionalized AFM tip from

dx.doi.org/10.1021/la502777h | Langmuir 2015, 31, 299−306

Aβ fibrils and protofibril films. Gold coated silicon nitride cantilevers were functionalized with isomers i_0 to i_2 as described in Experimental Methods. It is worth mentioning that the peptide sequence influences the degree of conjugation and stability of Au/tip−peptide conjugates, as well as their interactions with binding targets. For example, for AuNP conjugates, AuNP-i_0 and AuNP-i_2 peptide molecules on the gold surface have a surface packing of $\phi \approx 0.65$ molecule/nm^2; this is two times higher than that of AuNP-i_1 packing.[33,34] Thus, the same peptide packing ratio is expected for Au/tips-i_1 with respect to Au/tips-i_0, i_2. Figure 2 schematizes the experimental situation with respect to scales of interacting objects. The film profiles which are extracted from typical AFM profiles can be used to depict the substrate roughness with respect to the tip and peptide size. Enhancements in Figure 2 illustrate expected peptide orientations on the gold semisphere of the AFM tip as predicted by Guerrero et al.[34] for spherical AuNPs.

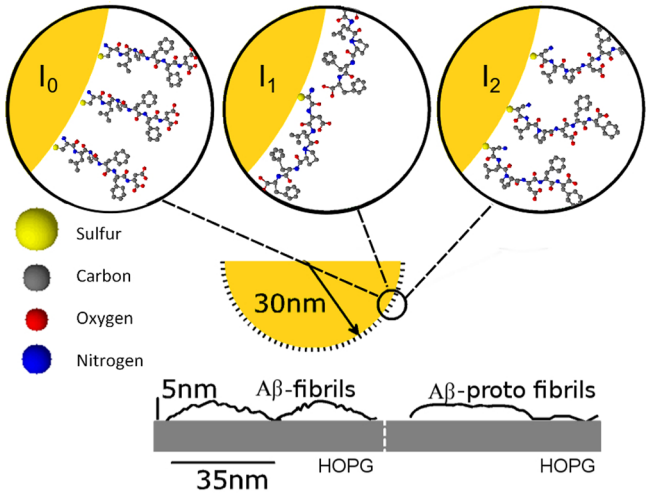

Figure 2. Diagram indicating the spatial conformation of peptide i_0, i_1, and i_2 on the colloidal probe surface. Colored bullets indicate distinct atoms on peptides. Typical measured profiles of Aβ fibrils as well as Aβ protofibrils films are indicated by solid lines to show the degree of roughness.

A detailed description of atomic force methods applied to surface characterization can be found in a recent review by Butt et al.[3] For our purposes, two approaches are available:[40] the Johnson−Kendall−Roberts (JKR) theory and the Derjaguin−Muller−Topolov (DMT) theory that relate the link between adhesion work, W_{ad}, and adhesion force, F_{ad}. Here, F_{ad} is defined as the pull-off force required to withdraw a spherical object of radius R from the planar surface. We noticed that the elastic deformation of surfaces is an important factor to relate W_{ad} to F_{ad}. Thus, for relatively high adhesive force in soft material the JKR theory states that

$$W_{ad} = \frac{2}{3\pi R} F_{ad} \tag{7}$$

For hard surfaces and weak adhesion, however, the DMT theory is more adapted to these conditions,[40] and it reads,

$$W_{ad} = \frac{1}{2\pi R} F_{ad} \tag{8}$$

Additionally, we explored the interactions of peptide conjugated tips with both Aβ protofibrils and well developed Aβ fibrils. Typical force curves on approach (upper panels) and retraction (lower panels) as a function on substrate deformation, D, are presented in Figure 3. For Aβ fibrils, force curves vary gradually with D, illustrating a relatively minor stiffness of fibrils. No difference in stiffness was observed between isomers (Figure 3a). The Hertz contact model was used to estimate the Young modulus as described by

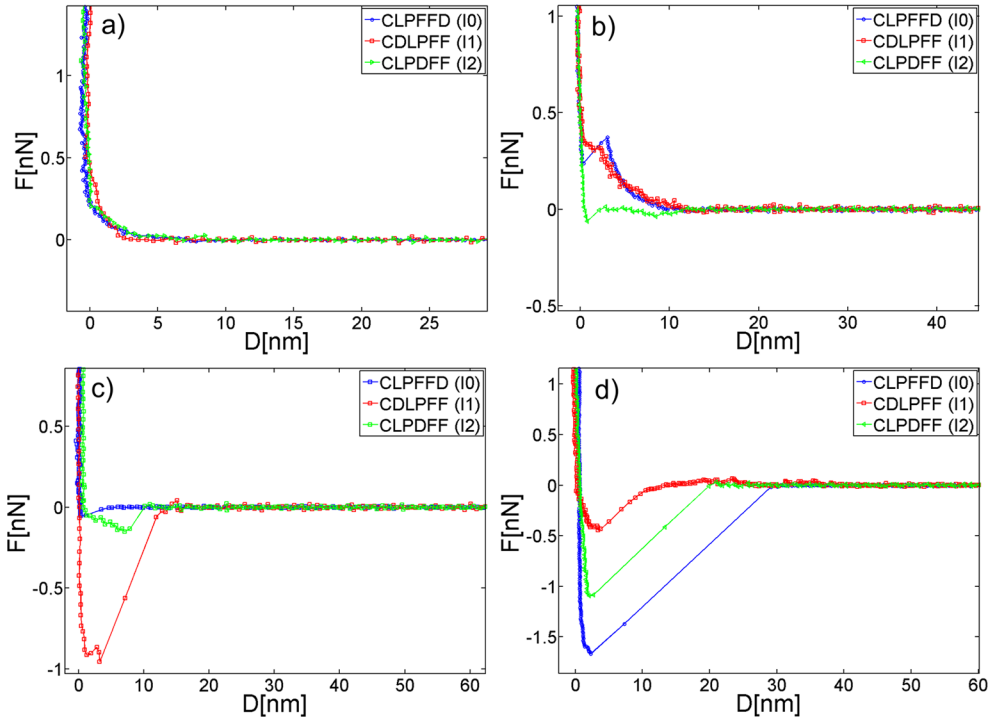

Figure 3. Typical force curves as a function of penetration D in approach (upper panels) and retraction (lower panels). Functionalized tips with i_0, i_1, and i_2 interacting with $A\beta_{1-42}$ well developed fibrils (a and c) and $A\beta_{1-42}$ protofibrils (b and d).

dx.doi.org/10.1021/la502777h | Langmuir 2015, 31, 299−306

Dimitriadis et al.[42] Typical values of the Young modulus of the Aβ fibrils were of the order of 230 ± 50 kPa. The force of adhesion, i.e., the force jump under retraction (Figure 3c), was, however, very different between isomers. In the case of protofibrils, the Young modulus was typically 500 ± 100 kPa, whereas the adhesion force was significantly higher compared to that of Aβ fibrils.

Because of the observed dispersion of adhesion force, which is related to the inherent probabilistic nature of our force measurements, we collected sufficient data curves to obtain representative adhesion force histograms. The process was carried out as follows: initially, a nearly homogeneous covered area of about 1 μm^2 was selected. It is scanned by translating the tip at steps of 50 nm. At each point, a force curve was acquired and analyzed. The process is repeated several times by selecting different regions of the substrates. We observed that there is no statistically significant aging of the tip. This is verified since the force statistic does not depend on whether it is performed with the first or the second half of the data. Nevertheless, in order to avoid contamination of the tips, the whole process is repeated several times with newly functionalized tips.

In Figure 4, we present histograms of adhesion work obtained for peptides (i_0, i_1, and i_2) interacting with proto fibrils and well developed Aβ fibrils. For protofibrils, the work of adhesion corresponding to the interaction with i_0 and i_2 was significantly higher with respect to i_1. This high interaction was predicted and attributed to the hydrophobic nature of protofibrils and the predominant exposition of hydrophobic residues in the functionalized tips with i_0 and i_2 with respect to i_1. In the case of the Aβ fibrils, i_0 and i_2 presented very low adhesion, which can be related to a more hydrophilic nature of Aβ fibrils with respect to protofibrils. However, i_1 presented a small but noticeable work adhesion. In Table 3, we summarize the average work of adhesion with its respective dispersion for peptides interacting with Aβ fibrils and protofibrils.

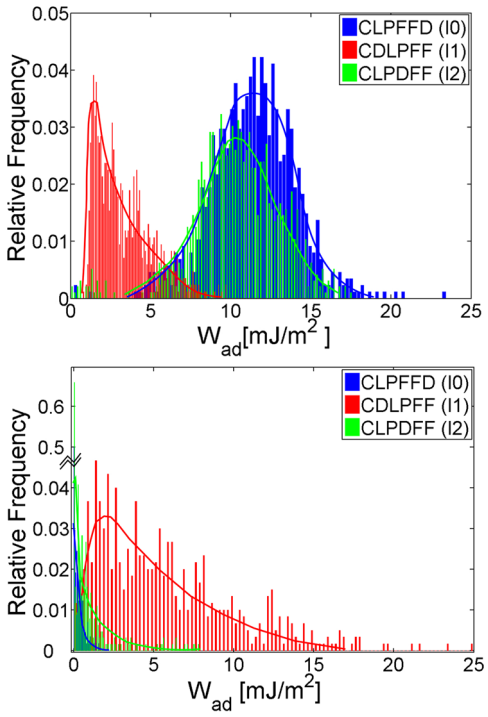

Figure 4. Adhesion work for protofibrils as well as fibrils of Aβ_{1-42} protein. (a) Histograms for the adhesion work of peptide i_0 (solid line: Gaussian), i_1 (solid line: Poisson), i_2 (solid line: Gaussian) to Aβ_{1-42} protofibrils. (b) Adhesion work of peptide i_0, i_1, and i_2 to Aβ_{1-42} fibrils. Solid lines are Poisson distributions.

Table 3. Work of Adhesion between Solid−Solid Interfaces As Measured by a Functionalized AFM Tip in Aqueous Solution

adhesion work (mJ/m^2)	$tipAu/i_0$	$tipAu/i_1$	$tipAu/i_2$	$tipAu$
HOPG-Aβ	0.2 ± 0.4	6 ± 2	0.4 ± 0.7	19 ± 11
HOPG-protofibrils	12 ± 2	3 ± 2	11 ± 2	6 ± 3

The distributions of adhesion work for i_0 and i_2 are nearly Gaussian, indicating that hydrophobic groups present in both peptides have a characteristic probability of encountering a similar group on the substrate at each trial. In other words, these peptides interact with Aβ protofibrils via specific hydrophobic sites with a nearly constant probability of occurrence. Thus, if we neglect correlation between the adhesion of peptides at distinct locations on the tip, the whole process can be modeled simply by a binomial distribution, where each trial is independent from one another. Defining the probability of adhesion of a single peptide as p, the probability for each peptide of not encountering an hydrophobic group is $1 - p$, and the probability of adhesion of m peptides groups onto the substrate reads

$$P(m, N_i, p) = \frac{N_i!}{m!(N_i - m)!} p^m (1 - p)^{N_i - m} \quad (9)$$

where the number of active peptides on the tip, N_i, is simply obtained by multiplying the packing fraction of peptide, ϕ_i, by the active surface, A_{cont}, of the tip in contact with the substrate. This is, $N_i \approx \phi_i A_{cont}$. By considering the penetration of the tip on the soft substrate, δ, the contact area is easily estimated to $A_{cont} \approx 2\pi R\delta$, which leads to $N_{i0} \approx N_{i2} \approx 370$, for $\delta \approx 3$ nm. It is worth noting that in the binomial distribution, the measured adhesion work average, $\langle W_{ad} \rangle$, and its respective variance, σ_W, are related with basic parameters as $\langle W_{ad} \rangle A_{cont} = \omega_i N_i p$ and $\sigma_W A_{cont} = \omega_i (N_i p(1-p))^{1/2}$, respectively, where ω_i is the adhesion energy per peptide. Thus, $\langle W_{ad} \rangle / \sigma_W = (N_i p/(1 - p))^{1/2}$. For i_0 and i_2 interacting with protofibrils, our measurements indicate that this ratio is about 6 and $\langle W_{ad} \rangle \approx$ 12 mJ/m^2, which leads to $p \approx 0.1$ and $\omega_i \approx 1.75 \times 10^{-19}$ J. However, for a molecule of radius R_m, the hydrophobic energy is estimated to $40R_m$ J/mol[43] (R_m is expressed in nm), which suggests that the effective size of hydrophobic groups in peptides i_0 and i_2 ranges from 1 to 2 nm, which is compatible with peptide size.

It is noteworthy that i_1 is the only Aβ peptide interacting in a similar manner with both Aβ fibrils as well as protofibrils. The fact that the hydrophilic component of Aβ fibrils dominates, which explains the low interaction of Aβ fibrils with i_0 and i_2 breakers, indicates that different functional groups of i_1 favor interactions with either Aβ proto fibrils or fibrils. To provide some quantitative understanding about this phenomenon, let us assume that due to the lower degree of functionalization of i_1, i_1 interacts with Aβ fibrils mediated by sites whose probability of occurrence is very small. This assumption is supported by the fact that the statistic of the work of addition for i_1 differs significantly from a Gaussian distribution, showing a marked

dx.doi.org/10.1021/la502777h | Langmuir 2015, 31, 299−306

asymmetry that is characteristic of a Poisson distribution. Thus, for $p \ll 1$, the distribution is assumed to be Poisson-like,

$$P(m, N_{i_1}p) = \frac{e^{-N_{i_1}p}}{m!}(N_{i_1}p)^m \quad (10)$$

where N_{i1} is the number of peptides i_1 on the active surface of the tip. For i_1, $\phi_{i1} \approx 0.32$, which leads to $N_{i1} \approx 180$. For the Poisson distribution, the average, $\langle W_{ad} \rangle$, and the variance, σ_W, produce $\langle W_{ad} \rangle\ A_{cont} = \omega_i N_{i1}p$ and $\sigma_W\ A_{cont} = \omega_i(N_{i_1}p)^{1/2}$, respectively. Using data in Table 3, we find, $\omega_{i1} \approx 12 \times 10^{-19}$ J and $N_{i1}p \approx 1$, which leads to $p \approx 5 \times 10^{-3}$, confirming our hypothesis that there is a very small probability of adhesion of i_1 but a relatively large interaction energy. The high value of the interaction energy suggests that either the hydrophobic group size is about 10 nm,[43] which is too large compared to the peptide size, or the interaction observed has a different origin. Since the coverage of peptide i_1 onto the gold surface is lower compared to that of i_0 and i_2, the second scenario seems more likely. Thus, the observed adhesion would be due to the interaction of patches of naked gold of the probe with fibrils and protofibrils.

CONCLUSIONS

By using the nanoprobe method, it is possible to put forward evidence of the hydrophobic nature of β-amyloid protofibrils and their interaction with the exposed hydrophobic residues of i_0 and i_2, which are positioned orthogonally with respect to the surface of the AFM tip. In contrast, amyloid fibrils which are less hydrophobic show a reduced proportion/number of interactions with all peptides onto the functionalized tip. Our results indicate that the orientation of the peptide on the surface and the degree of functionalization, which are dependent on the peptide sequence, are crucial parameters for the performance of the nanoprobe when interacting with the amyloid aggregates. Indeed, the nanoprobe functionalized with i_1 does not discriminate between amyloid fibrils and protofibrils, which we attributed to the low degree of functionalization.

Although protofibrils adsorbed on a graphite surface are more hydrophobic species than amyloid fibrils, there is no significant difference in the macroscopic behavior. On the contrary, the nanoprobe method allowed discrimination and identification of the hydrophobic/hydrophilic nature of β-amyloid aggregates.

Force spectroscopy and peptide functionalized nanoprobes represent a useful tool for a better understanding of nanobiointeractions and for the design of new functionalized nanoparticles to tune the interaction with amyloids, which are relevant for biomedical applications.

AUTHOR INFORMATION

Corresponding Authors

*(M.J.K.) E-mail: mkogan@ciq.uchile.cl.
*(F.M.) E-mail: francisco.melo@usach.cl.

Notes

The authors declare no competing financial interest.

ACKNOWLEDGMENTS

We are very grateful to Professor Fausto Sanz and Professor Helmut Coelfen for useful discussions. This research was supported by Conicyt Chile under grant Fondecyt Numbers 1130922 and 1130425 and Fondap 15130011 (to M.J.K.).

REFERENCES

(1) Israelachvili, J. *Intermolecular and Surface Forces*, 2nd ed.; Academic Press: London, 1991.
(2) Karshikoff, A. *Non-covalent Interactions in Proteins*, 1st ed.; Imperial College Press: London, 2006.
(3) Butt, H. J.; Cappella, B.; Kappl, M. Force measurements with the atomic force microscope: Technique, interpretation and applications. *Surf. Sci. Rep.* **2005**, *59*, 1−152.
(4) Butt, H. J. Measuring electrostatic, van der Waals, and hydration forces in electrolyte solutions with an atomic force microscope. *Biophys. J.* **1991**, *60*, 1438−1444.
(5) Butt, H. J. Measuring local surface charge densities in electrolyte solutions with a scanning force microscope. *Biophys. J.* **1992**, *63*, 578−582.
(6) Garcia-Manyes, S.; Gorostiza, P.; Sanz, F. Titration force microscopy on supported lipid bilayers. *Anal. Chem.* **2006**, *78*, 61−70.
(7) Kellermayer, M. S. Z. Visualizing and manipulating individual protein molecules. *Physiol. Meas.* **2005**, *26*, R119−R153.
(8) Bustamante, C.; Marko, J. F.; Siggia, E.; Smith, S. Entropic elasticity of lambda-phage DNA. *Science* **1994**, *265*, 1599−1600.
(9) Hugel, T.; Seitz, M. The study of molecular interactions by AFM force spectroscopy. *Macromol. Rapid Commun.* **2001**, *22*, 989−1016.
(10) Karsai, A.; Mártonfalvi, Z.; Nagy, A.; Grama, L.; Penke, B.; Kellermayer, M. S. Z. Mechanical manipulation of Alzheimer's amyloid β 1-42 fibrils. *J. Struct. Biol.* **2006**, *155*, 316−326.
(11) Lesné, S. E.; Sherman, M. A.; Grant, M.; Kuskowski, M.; Schneider, J. A.; Bennett, D. A.; Ashe, K. H. Brain amyloid-β oligomers in ageing and Alzheimer's disease. *Brain* **2013**, *136*, 1383−1398.
(12) Cohen, S.; Linse, S.; Luheshi, L. M.; Hellstrand, E.; White, D. A.; Rajah, L.; Otzen, D. E.; Vendruscolo, M.; Dobson, C. M.; Knowles, T. P. Proliferation of amyloid-β42 aggregates occurs through a secondary nucleation mechanism. *Proc. Natl. Acad. Sci. U.S.A.* **2013**, *110*, 9758−9763.
(13) Arimon, M.; Díez-Pérez, I.; Kogan, M. J.; Durany, N.; Giralt, E.; Sanz, F.; Fernández-Busquets, X. Fine structure study of Aβ1-42 fibrollogenesis with atomic force microscopy. *FASEB J.* **2005**, *7*, 10053−10063.
(14) Brambilla, D.; Droumaguet, B. L.; Nicolas, J.; Hashemi, S. H.; Wu, L.-P.; Moghimi, S. M.; Couvreur, P.; Andrieux, K. Nanotechnologies for Alzheimer's disease: diagnosis, therapy, and safety issues. *Nanomed., Nanotechnol. Biol. Med.* **2011**, *7*, 521−540.
(15) Linse, S.; Cabaleiro-Lago, C.; Xue, W.-F.; Lynch, I.; Lindman, S.; Thulin, E.; Radford, S. E.; Dawson, K. A. Nucleation of protein fibrillation by nanoparticles. *Proc. Natl. Acad. Sci. U.S.A.* **2007**, *104*, 8691−8696.
(16) Wei-hui, W.; Xun, S.; Ye-ping, Y.; Jia, H.; Lei, Z.; Qian, L.; Yu-fen, Z.; Yan-mei, L. TiO_2 nanoparticles promote β-amyloid fibrillation in vitro. *Biochem. Biophys. Res. Commun.* **2008**, *373*, 315−318.
(17) Vannoy, C. H.; Leblanc, R. M. Effects of DHLA-capped CdSe/ZnS quantum dots on the fibrillation of human serum albumin. *J. Phys. Chem. B* **2010**, *114*, 10881−10888.
(18) Zhang, D.; Neumann, O.; Wang, H.; Yuwono, V. M.; Barhoumi, A.; Perham, M.; Hartgerink, J. D.; Wittung-Stafshede, P.; Halas, N. J. Gold nanoparticles can induce the formation of protein-based aggregates at physiological pH. *Nano Lett.* **2009**, *9*, 666−671.
(19) Wagner, S. C.; Roskamp, M.; Pallerla, M.; Araghi, R. R.; Schlecht, S.; Koksch, B. Nanoparticle-induced folding and fibril formation of coiled-coil-based model peptides. *Small* **2010**, *6*, 1321−1328.
(20) Roberti, M. J.; Morgan, M.; Méndez, G.; Pietrasanta, L. I.; Jovin, T. M.; Jares-Erijman, E. A. Quantum dots as ultrasensitive nanoactuators and sensors of amyloid aggregation in live cells. *J. Am. Chem. Soc.* **2009**, *131*, 8102−8107.
(21) Skaat, H.; Shafir, G.; Margel, S. Acceleration and inhibition of amyloid-β fibril formation by peptide-conjugated fluorescent-maghemite nanoparticles. *J. Nanopart. Res.* **2011**, *13*, 3521−3534.
(22) Cabaleiro-Lago, C.; Quinlan-Pluck, F.; Lynch, I.; Lindman, S.; Minogue, A. M.; Thulin, E.; Walsh, D. M.; Dawson, K. A.; Linse, S.

Inhibition of amyloid β protein fibrillation by polymeric nanoparticles. *J. Am. Chem. Soc.* **2008**, *130*, 15437−15443.
(23) Xiao, L.; Zhao, D.; Chan, W.-H.; Choi, M. M.; Li, H.-W. Inhibition of beta 1-40 amyloid fibrillation with N-acetyl-l-cysteine capped quantum dots. *Biomaterials* **2010**, *31*, 91−98.
(24) Yoo, S. I.; Yang, M.; Brender, J. R.; Subramanian, V.; Sun, K.; Joo, N. E.; Jeong, S.-H.; Ramamoorthy, A.; Kotov, N. A. Innentitelbild: inhibition of amyloid peptide fibrillation by inorganic nanoparticles: functional similarities with proteins. *Angew. Chem., Int. Ed.* **2011**, *123*, 5096−5096.
(25) Thakur, G.; Micic, M.; Yang, Y.; Li, W.; Movia, D.; Giordani, S.; Zhang, H.; Leblanc, R. M. Conjugated quantum dots inhibit the amyloid β (1-42) fibrillation process. *Int. J. Alzheimer's Dis.* **2011**, *2011*.
(26) Mahmoudi, M.; Akhavan, O.; Ghavami, M.; Rezaee, F.; Ghiasi, S. M. A. Graphene oxide strongly inhibits amyloid beta fibrillation. *Nanoscale* **2012**, *4*, 7322−7325.
(27) Li, M.; Yang, X.; Ren, J.; Qu, K.; Qu, X. Using graphene oxide high near-infrared absorbance for photothermal treatment of Alzheimer's disease. *Adv. Mater.* **2012**, *24*, 1722−1728.
(28) Liao, Y.-H.; Chang, Y.-J.; Yoshiike, Y.; Chang, Y.-C.; Chen, Y.-R. Negatively charged gold nanoparticles inhibit Alzheimer's amyloid-β fibrillization, induce fibril dissociation, and mitigate neurotoxicity. *Small* **2012**, *8*, 3631−3639.
(29) Palmal, S.; Maity, A. R.; Singh, B. K.; Basu, S.; Jana, N. R.; Jana, N. R. Inhibition of amyloid fibril growth and dissolution of amyloid fibrils by curcumingold nanoparticles. *Chem.—Eur. J.* **2014**, *20*, 6184−6191.
(30) Soto, C.; Sigurdsson, E. M.; Morelli, L.; Kumar, R. A.; Castaño, E. M.; Frangione, B. β-Sheet breaker peptides inhibit fibrillogenesis in a rat brain model of amyloidosis: Implications for Alzheimer's therapy. *Nat. Med.* **1998**, *4*, 822−826.
(31) Kogan, M. J.; Bastus, N. G.; Amigo, R.; Grillo-Bosch, D.; Araya, E.; Turiel, A.; Labarta, A.; Giralt, E.; Puntes, V. F. Nanoparticle-mediated local and remote manipulation of protein aggregation. *Nano Lett.* **2006**, *6*, 110−115.
(32) Araya, E.; Olmedo, I.; Bastus, N.; Guerrero, S.; Puntes, V.; Giralt, E.; Kogan, M. Gold nanoparticles and microwave irradiation inhibit beta-amyloid amyloidogenesis. *Nanoscale Res. Lett.* **2008**, *3*, 435−443.
(33) Sigurdsson, E. M.; Permanne, B.; Soto, C.; Wisniewski, T.; Frangione, B. In vivo reversal of amyloid-β lesions in rat brain. *J. Neuropathol. Exp. Neurol.* **2000**, *59*, 11−17.
(34) Guerrero, A.; Adeva, A.; Caballero, L.; Melo, F.; Kogan, M. Exploring the surface charge on peptide-gold nanoparticle conjugates by force spectroscopy. *Langmuir* **2010**, *26*, 12026−12032.
(35) Olmedo, I.; Araya, E.; Sanz, F.; Medina, E.; Arbiol, J.; Toledo, P.; Alvarez-Lueje, A.; Giralt, E.; Kogan, M. J. How changes in the sequence of the peptide CLPFFD-NH_2 can modify the conjugation and stability of gold nanoparticles and their affinity for β-amyloid fibrils. *Bioconjugate Chem.* **2008**, *19*, 1154−1163.
(36) Hutter, J. L.; Bechhoeffer, J. Calibration of atomic-force microscope tips. *Rev. Sci. Instrum.* **1993**, *64*, 1868−1873.
(37) Kowalewski, T.; Holtzman, D. In situ atomic force microscopy study of Alzheimer's β-amyloid peptide on different substrates: New insights into mechanism of β-sheet formation. *Proc. Natl. Acad. Sci. U.S.A.* **1999**, *96*, 3688−3693.
(38) Wang, Z.; Zhou, C.; Wang, C.; Wan, L.; Fang, X.; Bai, C. AFM and STM study of β-amyloid aggregation on graphite. *Ultramicroscopy* **2003**, *97*, 73−79.
(39) Carré, A. Polar interactions at liquid/polymer interfaces. *J. Adhesion Sci. Technol.* **2007**, *21*, 961−981.
(40) Cho, J. H.; Lee, D. H.; Lim, J. A.; Cho, K.; Je, J. H.; Yi, J. M. Evaluation of the adhesion properties of inorganic materials with high surface energies. *Langmuir* **2004**, *20*, 10174−10178.
(41) Wang, S.; Zhang, Y.; Abidi, N.; Cabrales, L. Wettability and surface free energy of graphene films. *Langmuir* **2009**, *25*, 11078−11081.
(42) Dimitriadis, E. K.; Horkay, F.; Maresca, J.; Kachar, B.; Chadwick, R. S. Determination of elastic moduli of thin layers of soft material using the atomic force microscope. *Biophys. J.* **2002**, *82*, 2798−2810.
(43) Israelachvili, J.; Pashley, R. The hydrophobic interaction is long range, decaying exponentially with distance. *Nature* **1982**, *300*, 341−342.